Toward Early Stopping Detection for Non-Binary c-VEP-based BCIs: A Pilot Study

Víctor Martínez-Cagigal[1,2][0000−0002−3822−1787], Eduardo Santamaría-Vázquez[1,2][0000−0002−7688−4258], and Roberto Hornero[1,2][0000−0001−9915−2570]

[1] Biomedical Engineering Group (GIB), E.T.S. Ingenieros de Telecomunicación, University of Valladolid, Paseo de Belén, 15, Valladolid, 27011, Spain
[2] Centro de Investigación Biomédica en Red en Bioingeniería, Biomateriales y Nanomedicina (CIBER-BBN), Spain
victor.martinez.cagigal@uva.es

Abstract. Code-modulated visual evoked potentials (c-VEPs) have potential as a reliable and non-invasive control signal for brain-computer interfaces (BCIs). However, these systems need to become more user-friendly. Non-binary codes have been proposed to reduce visual fatigue, but there is still a lack of adaptive methods to shorten trial durations. To address this, we propose a nonparametric early stopping algorithm for the non-binary circular shifting paradigm. The algorithm analyzes the distribution of unattended commands' correlations and stops stimulation when the most probable correlation is considered an outlier. This proposal was evaluated offline with 15 healthy participants using p-ary maximal length sequences encoded with shades of gray. Results showed that the algorithm could stop stimulation in under two seconds for all sequences, achieving mean accuracies over 95%. The highest performances were achieved by bases $p = 2$ and $p = 5$, attaining 98.3% accuracy with ITRs of 164.8 bpm and 121.7 bpm, respectively. The proposed algorithm reduces required cycles without compromising accuracy for c-VEP-based BCI systems.

Keywords: Early stopping · non-binary codes · code-modulated visual evoked potential (c-VEP) · brain–computer interface (BCI) · electroencephalography (EEG).

1 Introduction

Non-invasive brain-computer interface (BCI) systems have the capability of interpreting users' intentions directly from their electroencephalographic (EEG) signals and converting them into commands for controlling external devices or applications [13]. However, decoding such intentions is challenging and requires the use of control signals that generate measurable responses in the EEG. These control signals can be generated either by processing external stimuli (exogenous approach) or by performing cognitive tasks (endogenous approach) [13].

Among other exogenous signals, code-modulated visual evoked potentials (c-VEPs) stand out as a promising strategy to develop non-invasive BCIs with high accuracy and speed [7].

In the most common paradigm, known as circular shifting, selectable commands flicker following uncorrelated shifted versions of a binary pseudorandom sequence [7]. In real-time, the identification of the desired command is determined by analyzing the correlation between the EEG response and these shifted templates [7]. Despite the excellent performances, several studies have reported that the high-contrast changes produced by binary codes, which use black and white flashes to encode commands, may cause visual fatigue for some users [5,4,12]. In a previous study, we proposed the use of non-binary sequences encoded with different shades of gray to improve user friendliness [6]. The results indicated that these non-binary codes are suitable for achieving high speed and accuracy while reducing visual fatigue.

Although c-VEP-based BCIs have great potential, they need to be further adapted to become more user-friendly technologies. Apart from addressing the visual fatigue, the adoption of adaptive methods to reduce as much as possible the trial decoding duration has been also identified as a current challenge in the literature [7]. In this sense, early stopping techniques that adaptively stop visual stimulation whenever the BCI is ready to deliver a command selection are still limited. Many of the previous approaches are incompatible with the circular shifting paradigm [9,11], require parameter optimization, or are dependent on the classifier stage [2,3]. Furthermore, none of these methods have been applied to non-binary stimulation.

The aim of this pilot study is to present a new nonparametric early stopping technique that is applicable to non-binary c-VEP-based BCIs. The method was offline tested with 5 different sequences of bases 2, 3, 5, 7 and 11; displayed at a rate of 120 Hz. The base indicates the number of distinct events that are encoded within the m-sequence, represented as a shades of gray. For instance, a base of 2 (i.e., binary) is encoded using solely black and white; whereas a base of 11 uses black, white, and an additional nine intermediate shades of gray [6]. Our algorithm is noteworthy due to its classifier-independence (filter-based), lack of need for parameter training (nonparametric), and ability to be implemented in real-time without being trained with additional EEG recordings. Moreover, to the best of our knowledge, this is the first early stopping method for non-binary visual stimulation based on the circular shifting paradigm.

2 Signals

We conducted our study using an offline database consisting of 15 healthy participants (mean age: 28.80 $\pm$ 5.02 years, 10 males, 5 females), who performed BCI spelling tasks using the "P-ary c-VEP Speller" application of MEDUSA©, which is publicly available at www.medusabci.com [10]. Prior to their participation, all users provided informed consent. EEG data was collected using a *g.USBamp* device (g.Tec, *Guger Technologies*, Austria) and recorded from 16

Table 1. Details regarding the generation of the p-ary m-sequences.

	Base	**Order**	**Length (bits)**	**Polynomial**	**Duration*** **(s/cycle)**
GF(2^6)	2	6	63	$x^6 + x^5 + 1$	0.525
GF(3^4)	3	4	80	$x^4 + 2x^3 + 1$	0.667
GF(5^3)	5	3	124	$3x^3 + 2x^2 + 1$	1.033
GF(7^2)	7	2	48	$4x^2 + 1$	0.400
GF(11^2)	11	2	120	$3x^2 + x + 1$	1.000

* Computed using a monitor refresh rate of 120 Hz.

active channels: F3, Fz, F4, C3, Cz, C4, CPz, P3, Pz, P4, PO7, POz, PO8, Oz, I1 and I2. The EEG device was grounded at AFz and referenced to the right earlobe. Visual stimuli were presented on a LED FullHD @ 144 Hz monitor (KEEP OUT XGM24F+ 23.8"), with a refresh rate of 120 Hz. A computer with an Intel Core i9-11900KF 3.5 GHz processor and 64 GB of RAM (Windows 10 OS) was used to display the visual stimuli. For additional details, refer to [6].

3 Methods

3.1 Paradigm

The circular shifting paradigm relies on the use of shifted versions of a pseudorandom sequence to encode individual commands. Therefore, it is crucial that the sequence exhibits low autocorrelation to facilitate subsequent decoding [7]. Maximal length sequences (i.e., m-sequences) are pseudorandom time series that demonstrate almost optimal autocorrelation properties, and can be generated by linear-feedback shift registers (LFSR). M-sequences are determined by: (1) the base p, i.e. the number of levels (e.g., $p = 2$ for binary m-sequences); (2) the order r, i.e. the number of LFSR taps; and (3) the generator polynomial expressed as a Galois Field of p elements, GF(p^r), i.e. the arrangement of the LFSR taps [1]. Apart from other mathematical constraints, the length of p-ary m-sequences is exactly $N = p^r - 1$ bits, and it is repeated cyclically [6]. Since commands are encoded with shifted versions of the p-ary m-sequences, the length of the sequence is directly related to the number of commands that can be encoded with the same code.

In this study, we utilized five distinct p-ary m-sequences with different bases, including binary GF(2^6) with base 2, GF(3^5) with base 3, GF(5^3) with base 5, GF(7^2) with base 7, and GF(11^2) with base 11. The detailed characteristics of each code, such as their length and duration when presented at a 120 Hz rate, are presented in Table 1. The paradigm consisted of a 16-command speller with adequately spaced lags to prevent any misclassifications. It is worth noting that a deterministic algorithm was utilized to avoid spurious correlations, as non-binary ($p > 2$) m-sequences exhibit periodic phase shifts that lead to high anti-/correlations. Additional information about this procedure can be found in

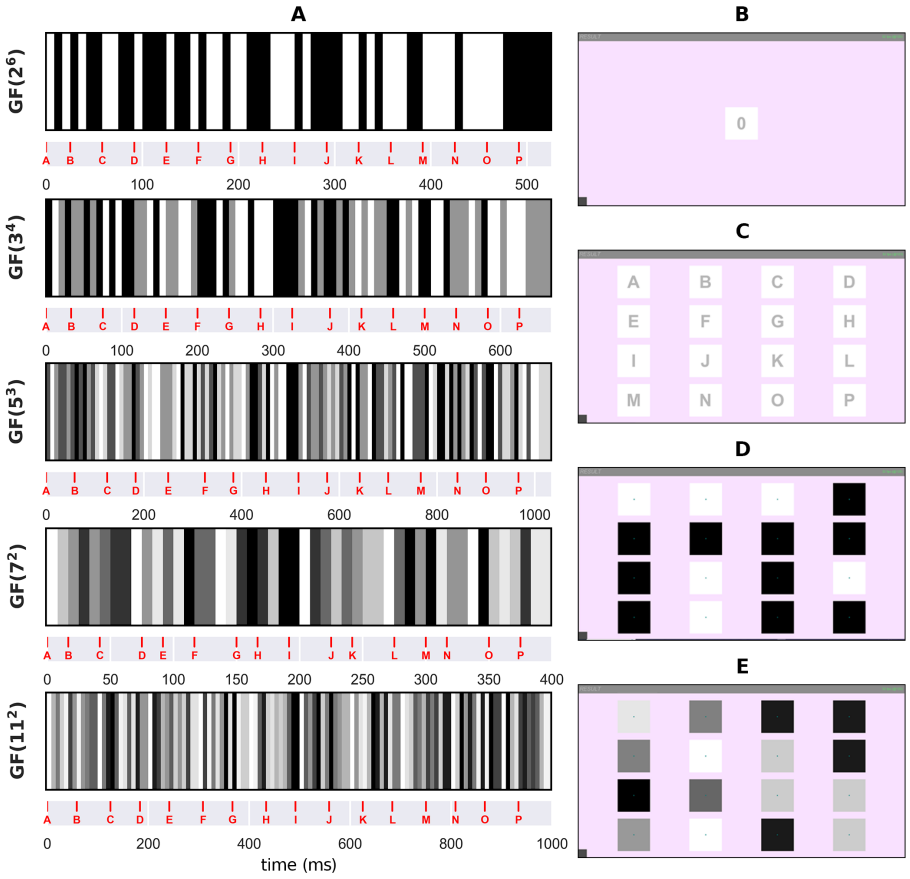

Fig. 1. (A) Gray encoding of each p-ary m-sequence and associated lags for each command. From top to bottom: base 2, base 3, base 5, base 7, and base 11. (B) Calibration stage, where a single command flashes according to the original p-ary m-sequence. (C) Online stage, showing the alphabetical arrangement of the 16 commands. (D) Snapshot of the binary m-sequence, GF(2^6). (E) Snapshot of the GF(11^2) m-sequence.

[6]. Figure 1 depicts the associated lags for each command, the arrangement of commands, and the gray encoding of each p-ary m-sequence, as well as several snapshots of the application [10].

3.2 Signal processing

In the calibration stage, the participant is instructed to focus on a single command encoded by the original p-ary m-sequence without lag, for a duration of k cycles. First, the EEG signal is preprocessed by a filter bank of bandpass filters (1-60 Hz, 12-60 Hz, and 30-60 Hz) and a notch filter at 50 Hz, generating three filtered EEG signals. For each signal, two versions of the EEG response are com-

puted: (1) the concatenated epochs, $\boldsymbol{A} \in \mathbb{R}^{[kN_s \times N_c]}$; and (2) the epochs averaged over the k cycles, $\boldsymbol{B} \in \mathbb{R}^{[N_s \times N_c]}$. Here, N_s represents the number of samples of a cycle, and N_c represents the number of channels. Subsequently, a canonical correlation analysis (CCA) is trained to find the spatial filter $\boldsymbol{\omega}_b$ that maximizes the correlation between the projected versions of $\boldsymbol{A}$ and $\boldsymbol{B}$. In this procedure, $\boldsymbol{B}$ is replicated k times to match the dimensions of $\boldsymbol{A}$. The main template (i.e., for the command without lag) is computed by projecting the averaged signal with the spatial filter $\boldsymbol{\omega}_b$, resulting in $\boldsymbol{x}_0 = \boldsymbol{B}\boldsymbol{\omega}_{\boldsymbol{b}}$. Templates for the other commands are calculated by circularly shifting this main template based on their corresponding lags. After this process, 16×3 templates, each for a command and filtered signal, are obtained. It is worth noting that calibration epochs with a standard deviation that is three times greater than the average standard deviation of all epochs were discarded before training the CCA [6]. A raster latency correction was applied to the trained templates, following the recommendation of Nagel et al. (2018) [8].

During online mode, a similar approach is applied to identify the command at which the user is looking in real-time. EEG signal is preprocessed, and individual epochs are averaged and projected using the spatial filter $\boldsymbol{\omega}_b$. The correlation between the resulting projection and all templates is then computed, yielding $\hat{\boldsymbol{\rho}} \in \mathbb{R}^{16\times 3}$. After averaging across the filtered signals, $\boldsymbol{\rho} \in \mathbb{R}^{16\times 1}$ is obtained. The index of the selected command corresponds to the one that yields the highest correlation value, i.e., $\arg\max_i(\boldsymbol{\rho})$ [7].

3.3 Proposed early stopping method

The purpose of an effective early stopping method is to select a command before a fixed number of cycles have elapsed, enabling real-time adaptation of the signal processing pipeline to the characteristics of the EEG signal. In a hypothetical scenario, the selection of a command is expected to take more time when the user is slightly distracted or when the EEG is contaminated with artifacts, and less time under ideal conditions. Importantly, a trial is no longer composed of a fixed number of cycles, but rather a variable number of cycles. Thus, the early stopping algorithm must make a binary decision each time a cycle is fully displayed: (1) select the most probable command; or (2) continue the visual stimulation for one additional cycle.

As detailed in Section 3.2, the online signal processing pipeline calculates a comparison between the EEG response from the start of the trial to the end of the current cycle and the command templates, resulting in a correlation vector $\boldsymbol{\rho} \in \mathbb{R}^{16\times 1}$. After arranging this vector in descending order, ρ_1 corresponds to the most likely command as it represents the highest correlation. The remaining correlations, $\rho_2, \rho_3, \ldots, \rho_{16}$, can be considered as spurious correlations associated with non-attended commands. Additionally, we can widen the number of observations of spurious correlations by computing the correlation of the EEG response with all possible shifted versions of the template, not just with those lags associated to the selectable commands. We end up with a correlation vector of length N, where N is the length of the p-ary m-sequence. Thus, ρ_1 corresponds

to the selected command, and $\boldsymbol{\rho}_{spu} = [\rho_2, \ldots, \rho_N]$ constitutes the distribution of spurious correlations. A reliable approach to determining whether ρ_1 indeed corresponds to the attended command would be to verify whether it is an outlier from the distribution $\boldsymbol{\rho}_{spu}$ (i.e., its correlation is statistically higher than that of the presumable non-attended commands).

Various techniques can be used to detect outliers from distributions, including those based on hypothesis testing or on the interquartile range. In this study, we suggest employing z-scores due to their simplicity. Assuming that the spurious distribution is normal, i.e., $\boldsymbol{\rho}_{spu} \sim \mathcal{N}(\mu, \sigma)$, we can identify ρ_1 as an outlier if $\rho_1 - \mu > h\sigma$, where $h = 3$. Thus, we can ascertain that ρ_1 is an outlier if it exceeds the 99.87% percentile of the spurious distribution. Consequently, if ρ_1 is an outlier, the command selection is delivered; otherwise, the visual stimulation continues with the next cycle.

3.4 Evaluation protocol

This pilot study entailed an exploratory analysis of offline data gathered from 15 healthy participants who completed spelling tasks utilizing a 16-command c-VEP speller, which was encoded with the p-ary m-sequences GF(2^6), GF(3^5), GF(5^3), GF(7^2), GF(11^2). Specifically, a total of 300 calibration cycles (6 runs $\times$ 5 trials $\times$ 10 cycles) and 320 test cycles (2 runs $\times$ 16 trials $\times$ 10 cycles) per participant were acquired for each p-ary m-sequence. During the test cycles, participants selected all commands in alphabetical order twice [6].

4 Results and discussion

4.1 Correlation distributions

Figure 2 depicts the correlations for the selected commands ρ_1, as well as for the non-attended ones $\boldsymbol{\rho}_{spu}$. Results obtained from the Kolmogorov-Smirnov test reveal that all distributions (ρ_1 and $\boldsymbol{\rho}_{spu}$ for both calibration and test data) are normal (p-value < 0.01). Given that the normality assumption is satisfied for the z-score, the estimated value of 99.87% can be considered accurate. Moreover, a significant similarity in the distributions between calibration and test data (p-value < 0.01, Wilcoxon-signed rank test) indicates the potential for optimizing h using only calibration data without acquiring additional recordings. It is worth noting that an increase in the number of cycles results in a greater separation between ρ_1 and $\boldsymbol{\rho}_{spu}$ distributions. This phenomenon highlights the tradeoff between speed and accuracy. For instance, stopping in the very early cycles poses a higher risk of misclassification, but it allows for a faster selection speed.

4.2 Performance analysis

Table 2 displays the performance results, including accuracy and number of cycles, of each participant and p-ary m-sequence. The theoretical maximum accuracy, i.e. the minimum number of cycles required to achieve the highest accuracy

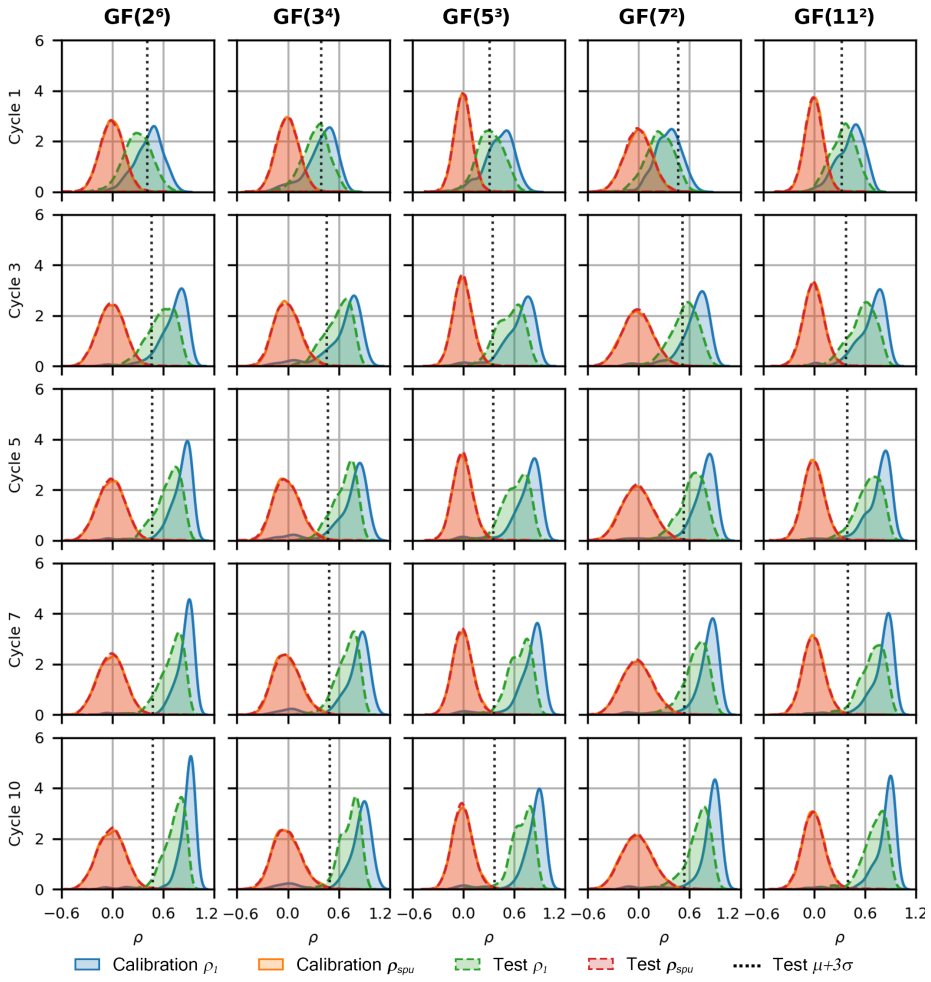

Fig. 2. Distribution of the correlations of the selected commands, ρ_1; and the spurious distributions $\boldsymbol{\rho}_{spu}$ for all p-ary m-sequences. Both calibration (blue and orange) and test (green and red) distributions are shown, including the estimated 99.87% percentile in test. Only cycles 1, 3, 5, 7 and 10 are depicted for visualization purposes.

(equivalent to 10 cycles in this database), is also included for comparison purposes. As shown, the mean visual stimulation duration of all p-ary m-sequences is below 2 seconds, with all sequences achieving accuracies exceeding 95%. The top performances sorted by accuracy are as follows: 98.3% with 1.8 cycles for GF(5^3), 98.3% with 2.6 cycles for GF(2^6), 98.1% with 2.4 cycles for GF(3^4), 98.1% with 1.8 cycles for GF(11^2), and 95.6% with 4.1 cycles for GF(7^2). Additionally, the mean information transfer rates (ITR) range from 121.7 to 164.8

Table 2. Offline results applying early stopping with all p-ary m-sequences

	GF(2^6)				**GF**(3^4)				**GF**(5^3)				**GF**(7^2)				**GF**(11^2)			
	E.S.		T.M.		E.S.		T.M.		E.S.		T.M.		E.S.		T.M.		E.S.		T.M.	
	%	N_c	%	N_c	%	N_c	%	N_c	%	N_c	%	N_c	%	N_c	%	N_c	%	N_c	%	N_c
U01	100	1.7	100	1.2	100	1.8	100	1.2	100	1.3	100	1.2	96.9	3.1	100	1.7	100	1.4	100	1.1
U02	100	2.2	100	1.3	100	1.9	100	1.1	100	1.2	100	1.0	96.9	3.6	100	1.8	100	1.5	100	1.2
U03	100	3.1	100	1.2	96.9	1.3	100	1.1	100	1.6	100	1.0	100	2.5	100	1.2	100	1.2	100	1.1
U04	100	2.0	100	1.1	100	1.5	100	1.0	100	1.1	100	1.0	100	8.2	100	1.4	100	1.1	100	1.0
U05	96.9	2.8	100	1.8	100	3.7	100	1.6	100	1.8	100	1.3	93.8	5.0	96.9	2.0	100	1.5	100	1.1
U06	100	2.5	100	1.6	100	2.7	100	1.4	96.9	1.3	100	1.2	100	3.0	100	1.8	100	1.7	100	1.1
U07	100	2.6	100	1.4	100	1.5	100	1.1	100	1.7	100	1.2	93.8	2.4	100	1.6	100	1.7	100	1.1
U08	100	2.2	100	1.2	100	1.3	100	1.1	100	1.8	100	1.1	96.9	3.0	100	1.7	100	1.3	100	1.0
U09	100	1.8	100	1.2	100	2.0	100	1.2	100	1.6	100	1.3	100	2.6	100	1.3	78.1	3.9	84.4	2.5
U10	100	2.2	100	1.3	100	1.6	100	1.1	100	1.4	100	1.0	100	2.7	100	1.7	100	1.1	100	1.0
U11	96.9	4.1	96.9	2.1	84.4	4.3	90.6	2.7	81.2	4.2	93.8	2.2	75.0	8.4	90.6	3.4	100	3.0	100	1.3
U12	96.9	4.2	96.9	2.0	93.8	3.0	100	1.7	96.9	2.8	100	1.9	96.9	6.2	100	2.4	96.9	1.9	100	1.3
U13	93.8	1.9	100	1.3	100	2.0	100	1.0	100	1.1	100	1.1	96.9	3.0	100	1.4	100	1.3	100	1.1
U14	90.6	4.2	100	2.2	96.9	4.8	100	2.2	100	2.5	100	1.6	90.6	4.6	100	2.4	96.9	2.9	100	1.6
U15	100	2.3	100	1.3	100	2.3	100	1.3	100	2.0	100	1.2	96.9	2.8	100	1.5	100	1.4	100	1.1
avg.	**98.3**	**2.6**	99.6	1.5	**98.1**	**2.4**	99.4	1.4	**98.3**	**1.8**	99.6	1.3	**95.6**	**4.1**	99.2	1.8	**98.1**	**1.8**	99.0	1.2
std.	2.8	0.8	1.1	0.3	4.1	1.1	2.3	0.5	4.7	0.8	1.6	0.3	6.1	1.9	2.4	0.5	5.4	0.8	3.9	0.4
ITR	**164.8**		170.5		**143.3**		148.2		**121.7**		125.9		**131.6**		143.7		**126.9**		129.6	
dur.	**1.4 s**		0.8 s		**1.6 s**		0.9 s		**1.9 s**		1.3 s		**1.6 s**		0.7 s		**1.8 s**		1.2 s	

E.S.: early stopping, T.M.: theoretical maximum (minimum number of cycles to attain the accuracy that would have been obtained using 10 cycles), %: accuracy, N_c: number of cycles, avg.: average, std.: standard deviation, ITR: mean information transfer rate in bit per minute (bpm), dur.: mean duration of the visual stimulation in seconds.

bpm. These findings suggest that the proposed early stopping algorithm can deliver fluent command selection while achieving high accuracy.

As could be expected, the shortest m-sequence, GF(7^2), yielded the lowest accuracy (95.6%). Figure 1 indicates that the ρ_1 and $\boldsymbol{\rho}_{spu}$ distributions overlapped more in this m-sequence than in the others, especially in the first cycle. While the average number of cycles for GF(7^2) is high relative to the others, which does not necessarily imply a longer trial duration, it would have been expected to be even higher to cope with this uncertainty. Therefore, individual optimization of h for each p-ary m-sequence could potentially benefit the system's performance, though further analyses are necessary to gain insight into this phenomenon.

The theoretical maximum accuracy suggests that trial duration could have been reduced to between 0.7-1.3 s, with accuracy exceeding 99% achievable through an ideal early stopping algorithm. This is equivalent to stopping between the first and second cycle. However, Figure 1 shows that the ρ_1 and $\boldsymbol{\rho}_{spu}$ distributions are difficult to separate in the first cycle, resulting in unreliable selections using our method. It remains an open question whether other approaches can reach this theoretical maximum. Interestingly, the increase in accuracy by the theoretical maximum is not significant by all p-ary m-sequences (p-value $>$ 0.05, Wilcoxon signed-rank test), except for the GF(7^2) m-sequence (p-value = 0.0036). Although we assert that our results demonstrate the usefulness of our algorithm, this observation indicates that there is still room for improvement.

4.3 Limitations and future lines of research

Despite the success of the proposed early stopping algorithm, there are still opportunities for enhancing its reliability. To begin with, it is crucial to conduct an online proof of concept and increase the sample size to improve the statistical power of the results. Additionally, it would be desirable to evaluate the algorithm's efficacy with motor-disabled participants. A promising research direction would be also to complement the algorithm with an asynchronous stage to monitor users' attention. Currently, the cumulative correlation across cycles presents a challenge in detecting a change from non-control to control cycles, as previous non-control epochs could negatively impact the correlation analysis. Therefore, an asynchronous algorithm could be focused on detecting attention in single cycles. Another possible avenue for investigation would be to explore whether an optimization of h between users or p-ary m-sequences could enhance the final classification.

5 Conclusions

This study introduces a novel early stopping algorithm for non-binary c-VEP-based BCIs, which presents a promising alternative for minimizing visual fatigue for end-users. The main strengths of this method are its classifier-independence, the lack of need for parameter training, and its real-time application without

requiring additional EEG recordings. In an offline analysis, the algorithm was found to reduce trial duration to less than 2 seconds while achieving over 95% accuracy for five different p-ary m-sequences, namely GF(2^6), GF(3^4), GF(5^3), GF(7^2), and GF(11^2). Although the algorithm's efficacy was demonstrated for all the tested m-sequences, the highest accuracy was achieved with GF(2^6) and GF(5^3), which attained 98.3% accuracy with 1.4 s and 1.9 s of stimulation, equivalent to ITRs of 164.8 bpm and 121.7 bpm, respectively. In conclusion, the proposed early stopping algorithm represents a valuable metric for significantly reducing the required number of cycles without compromising the system's accuracy in the circular shifting paradigm.

Acknowledgements This research was supported by projects TED2021-129915B-I00, RTC2019-007350-1 and PID2020-115468RB-I00 funded by MCIN/AEI/10.13039/501100011033 and 'European Union NextGenerationEU/PRTR'; and by 'Centro de Investigación Biomédica en Red en Bioingeniería, Biomateriales y Nanomedicina (CIBER-BBN)' through 'Instituto de Salud Carlos III' cofunded with European Regional Development Fund (ERDF) funds. E. Santamaría-Vázquez was in receipt of a PIF grant by the 'Consejería de Educación de la Junta de Castilla y León'.

References

1. Buračas, G.T., Boynton, G.M.: Efficient design of event-related fMRI experiments using m-sequences. NeuroImage **16**(3 I), 801–813 (2002). https://doi.org/10.1006/nimg.2002.1116
2. Gembler, F., Stawicki, P., Saboor, A., Benda, M., Grichnik, R., Rezeika, A., Volosyak, I.: A Dictionary Driven Mental Typewriter Based on Code-Modulated Visual Evoked Potentials (cVEP). In: Proceedings - 2018 IEEE International Conference on Systems, Man, and Cybernetics, SMC 2018. pp. 619–624. IEEE (2018). https://doi.org/10.1109/SMC.2018.00114
3. Gembler, F., Volosyak, I.: A novel dictionary-driven mental spelling application based on code-modulated visual evoked potentials. Computers **8**(2) (2019). https://doi.org/10.3390/computers8020033
4. Gembler, F.W., Rezeika, A., Benda, M., Volosyak, I.: Five Shades of Grey: Exploring Quintary m -Sequences for More User-Friendly c-VEP-Based BCIs. Computational Intelligence and Neuroscience **2020** (2020). https://doi.org/10.1155/2020/7985010
5. Ladouce, S., Darmet, L., Torre Tresols, J.J., Velut, S., Ferraro, G., Dehais, F.: Improving user experience of SSVEP BCI through low amplitude depth and high frequency stimuli design. Scientific Reports **12**(1), 1–12 (2022). https://doi.org/10.1038/s41598-022-12733-0
6. Martínez-Cagigal, V., Santamaría-Vázquez, E., Pérez-Velasco, S., Marcos-Martínez, D., Moreno-Calderón, S., Hornero, R.: Non-binary m-sequences for more comfortable brain-computer interfaces based on c-VEPs. Expert Systems with Applications (Accepted) (2023). https://doi.org/10.1016/j.eswa.2023.120815
7. Martínez-Cagigal, V., Thielen, J., Santamaría-Vázquez, E., Pérez-Velasco, S., Desain, P., Hornero, R.: Brain-computer interfaces based on code-modulated visual

evoked potentials (c-VEP): a literature review. Journal of Neural Engineering **18**(6), 061002 (2021). https://doi.org/10.1088/1741-2552/ac38cf
8. Nagel, S., Dreher, W., Rosenstiel, W., Spüler, M.: The effect of monitor raster latency on VEPs, ERPs and Brain–Computer Interface performance. Journal of Neuroscience Methods **295**, 45–50 (2018). https://doi.org/10.1016/j.jneumeth.2017.11.018
9. Nagel, S., Spüler, M.: World's fastest brain-computer interface: Combining EEG2Code with deep learning. PLoS ONE **14**(9), 1–15 (2019). https://doi.org/10.1371/journal.pone.0221909
10. Santamaría-Vázquez, E., Martínez-Cagigal, V., Marcos-Martínez, D., Rodríguez-González, V., Pérez-Velasco, S., Moreno-Calderón, S., Hornero, R.: MEDUSA©: A novel Python-based software ecosystem to accelerate brain-computer interface and cognitive neuroscience research. Computer Methods and Programs in Biomedicine **230**(107357) (2023). https://doi.org/10.1016/j.cmpb.2023.107357
11. Thielen, J., Marsman, P., Farquhar, J., Desain, P.: From full calibration to zero training for a code-modulated visual evoked potentials brain computer interface. Journal of Neural Engineering **18**(5), 56007 (2021). https://doi.org/10.1088/1741-2552/abecef
12. Wandell, B.A., Dumoulin, S.O., Brewer, A.A.: Visual field maps in human cortex. Neuron **56**(2), 366–383 (2007). https://doi.org/10.1016/j.neuron.2007.10.012
13. Wolpaw, J., Wolpaw, E.W.: Brain-computer interfaces: principles and practice. OUP USA (2012)